Available online at www.sciencedirect.com
SCIENCE DIRECT®
Catalysis Today 89 (2004) 35–45
CATALYSIS TODAY
www.elsevier.com/locate/cattod

Metal effect and flow rate effect in the hydrogen production from methane

Franz-Josef Spiess [a,1], Steven L. Suib [a,b,c,*], Kanji Irie [d], Yuji Hayashi [e], Hiroshige Matsumoto [f]

[a] *Department of Chemistry, University of Connecticut, U-60, Storrs, CT 06269-4060, USA*
[b] *Department of Chemical Engineering, University of Connecticut, Storrs, CT 06269-4060, USA*
[c] *Institute of Material Science, University of Connecticut, Storrs, CT 06269-4060, USA*
[d] *Daido Steel, Daido Steel Co. Ltd., 2-30 Daido-cho, Minami-ku, Nagoya 457-8545, Japan*
[e] *Fujitsu Laboratories Ltd., Kawasaki 852, Japan*
[f] *Nagasaki University, Nagasaki 852, Japan*

Abstract

The metal effect of the inner electrode used for the decomposition of methane and the resulting evolution of hydrogen by discharge plasmas was investigated. Several different electrodes were used in this study including noble metals such as palladium and other metals such as iron and copper. The noble metals showed the highest activity in methane decomposition and hydrogen production. Nickel and gold showed considerable deactivation, whereas the activity of iron decreased less. Coated electrodes with copper and tin oxide nanoparticles exhibited high activity in these reactions. The effect of the flow rate and the cleaning of the electrode were examined as further objectives of this study. The decomposition of methane and the evolution of hydrogen decreased with increasing flow rate in a negative exponential manner due to the lower residence time. The cleaning of the electrode has a profound effect on the conversions and allows one to observe the catalytic effect of the metal electrodes, which are otherwise covered by coke produced in the reaction. A mechanism was developed using data obtained from mass spectrometry and combined gas chromatography and mass spectrometry.

Keywords: Mass spectrometry; Chromatography; Nanoparticles

1. Introduction

Methane is the main component of natural gas. Methane (CH_4) and natural gas, the least CO_2-intensive of the fossil fuels, are used in a variety of different fields. Natural gas is used in residential applications for space and water heating and for cooking purposes. Natural gas can also be employed for air conditioning and the production of electricity by natural gas fuel cells. Commercially, natural gas is also important for heating and cooling, and is utilized in the food industry for cooking and food preparation. Natural gas powered generators and back-up generators are becoming used more and more in commercial and office buildings. Industry alone uses 43% of all natural gas [1]; in addition, natural gas is used for heating in the pulp and paper, metals, chemicals, petroleum refining, stone, clay and glass, plastic, and food processing industries. Useful applications include waste treatment and incineration, metal preheating (particularly for iron and steel), drying and dehumidification, glass melting, and fueling industrial boilers. Natural gas is a feedstock for the production of hydrogen, methanol and related chemicals, and is a source for the extraction of butane, ethane, and propane, which are applicable as feedstock in the fertilizer and pharmaceutical industries. Furthermore, natural gas is applied to a great extent for the generation of electricity in steam generating units for turbines. Natural gas powered vehicles have become more popular due to environmental concerns [1].

Methane is a very potent greenhouse gas and has a global warming potential 21 times that of carbon dioxide with an atmospheric concentration of 1721 ppb [2]. Its major sources

* Corresponding author. Present address: Institute of Material Science, University of Connecticut, Storrs, CT 06269-4060, USA.
Fax: +1-860-486-2981.
E-mail address: suib@uconnvm.uconn.edu (S.L. Suib).
[1] Present address: Institut für Physikalische Chemie, Universität Würzburg, Am Hubland, 97074 Würzburg, Germany.

0920-5861/$ – see front matter © 2003 Elsevier B.V. All rights reserved.
doi:10.1016/j.cattod.2003.11.043

are releases from natural gas and petroleum production, from rice paddies, waste dumps, and livestock [2]. Therefore, ways to reduce CO_2 emissions from natural gas are sought. The production of hydrogen from natural gas might be one alternative. In natural gas fuel cells, reformers (steam reformers, partial oxidation reformers, and auto-thermal reformers) produce internally the needed hydrogen for the electrochemical processes [3].

Traditionally, hydrogen was and still is produced by steam reforming of natural gas. This is done at temperatures between 500 and 800 °C employing $Ni/MgAl_2O_4$. This process is highly endothermic and requires considerable energy input for the vaporization of water and for heating the reaction [4]. Recently, this process has been used to steam reform biomasses such as organic waste using commercial multicomponent catalysts, which generally contain Ni, K, Ca, and Mg on alumina-based supports [5]. New partial oxidation catalysts for fuel cell applications were developed by Pino et al. [6] using ceria supported platinum catalysts showing hydrogen selectivities of over 90%.

Alternatively, hydrogen can be produced using solar irradiation and active photocatalysts [7–15]. Licht et al. [7,8] report the possibility of over 18% conversion of water by solar energy to hydrogen fuel based on calculations and experiments involving RuS_2 as one of the catalysts. Other materials such as oxide semiconductor photocatalysts such as doped $InTaO_4$ or TiO_2 (modified or in conjunction with sonication) have been investigated as well [9–11]. Miller and Rocheleau [12] developed multi-junction thin film photoelectrodes containing amorphous silicon or copper-indium-gallium-diselenide with expected solar to hydrogen conversions of over 10%. Mechano-catalytic methods and biological hydrogen from fuel gases and water are promising concepts as well [13]. T-Raissi [14] analyzed new hydrogen production technologies such as thermochemical H_2S reformation of methane with and without the use of a solar component and catalyzed micro-reformers for the decomposition of ammonia. Algae have been observed to produce hydrogen by photosynthesis and hydrogenase activity in the presence of background oxygen which inhibits hydrogen production at high levels [15].

Similar to the steam reforming process, processes have been developed using thermal and discharge plasmas to use natural gas to produce hydrogen [16–19]. Bromberg et al. [16] used thermal plasmas (several 1000 K) to produce up to 50% hydrogen in plasma reformers at 2–3 kW power input. Mutaf-Yardimci et al. [17] observed 16% conversion in the reforming of CO_2 and CH_4 in a pulsed corona discharge reactor after preheating the mixture thermally to 900 °C. Liu et al. [18] observed dielectric barrier discharges during diamond deposition using optical emission spectroscopy and reported the excitation temperature and various radical species. An atmospheric pressure glow plasma enhanced CVD system for simultaneous production of hydrogen and carbon nanotubes (CNTs) by direct methane decomposition was used by Nozaki et al. [19], employing methane/hydrogen/helium gas mixtures.

Our group performed various reactions involving reformation of CH_4 and CO_2. Brock et al. [20] used a Pt tubular and fan PACT reactor for this reaction, whereas Huang et al. [21] used a novel T-shaped tubular reactor with various electrode setups. This work studied the effect of using different metal electrodes on the hydrogen production from methane silent glow discharge plasmas.

2. Experimental

2.1. Preparation of gas mixtures

Methane used in these experiments was obtained from commercial vendors such as Airgas. Its purity was of CP grade (99.5% pure). The content of the feed gas is just a feed of pure methane at room temperature and atmospheric pressure. The flow rates used ranged over 5–250 ml/min for the plasma reactions at normal temperature and pressure. Ultrahigh purity air, also acquired from Airgas (moisture less than 5 ppm), was used to purge the reactors to remove some of the coke deposits that form typically in these reactions. Purges were done overnight in some cases.

2.2. Tubular reactor setup

The reactions were carried out with a plasma and catalysis integrated technologies (PACT) tubular reactor with exchangeable electrode. This reactor is depicted in Fig. 1. The reactor consisted of an exchangeable electrode of 10 cm length and 8 mm outer diameter (an example of which is the Pd electrode shown in Fig. 2a), a quartz tube of 15 cm length and 10 mm inner and 12 mm outer diameter acting as a dielectric separating outer and inner electrodes, and aluminum foil of 10 cm wrapped around this outer electrode. The exchangeable electrode consists of the electrode itself

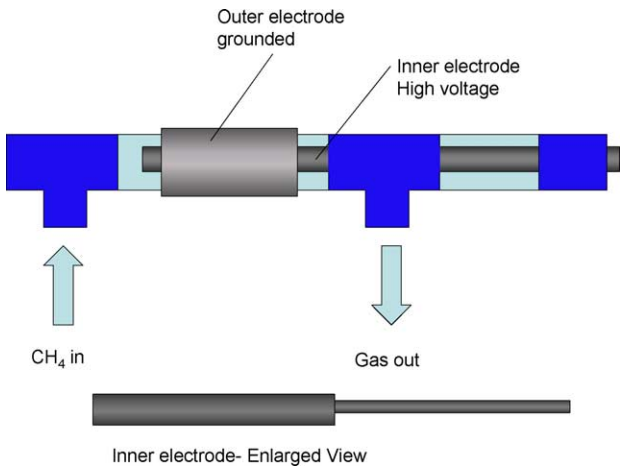

Fig. 1. Reactor setup for exchangeable electrodes in methane reactions.

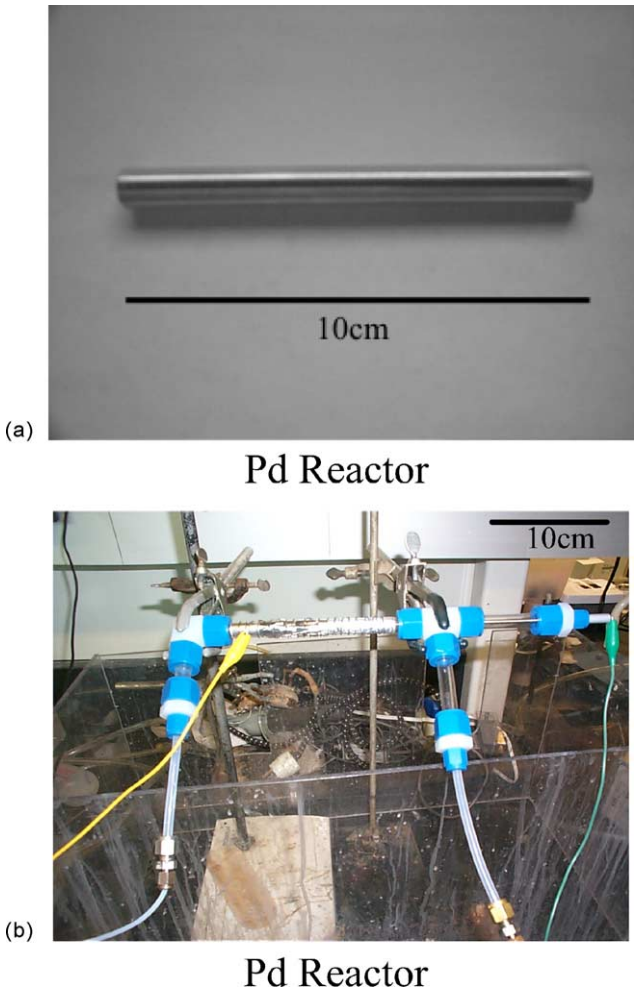

Fig. 2. (a) Exchangeable electrode, example of a Pd electrode and (b) photograph of Pd electrode setup.

and a metal rod onto which this electrode was screwed. Various materials such as gold and rhodium were electroplated onto a copper rod at a thickness of 100 μm and used as electrodes. The metal rod was of 15 cm length and 2 mm outer diameter. This metal rod was in a glass tube of the same diameters as the quartz tube and 7 cm in length and held in place by Swagelok fittings. The exposed end of this metal rod (outside of the Swagelok fitting) was used as the electric contact for the inner electrode to the high voltage source.

2.3. Reaction and circuit setup

The setup used in these reactions is shown in Fig. 2b. The reaction gas methane was introduced at room temperature and atmospheric pressure into the tubular reactor, and its flow was adjusted by an in-line rotameter with a set flow rate of 20 ml/min in most experiments. In another study, the flow rate was altered between 10 and 200 ml/min to investigate the flow rate dependence of the conversion. The system was

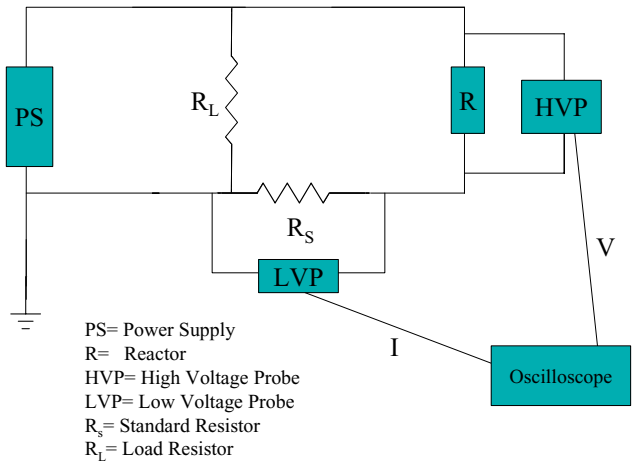

Fig. 3. Circuit diagram for the tubular plasma reactor.

equilibrated at the beginning of a run, and then the power supply was turned to the desired level and continued until equilibrium was achieved.

The circuit design in these experiments is identical to the one shown in Fig. 3. The high voltage was generated by an UHV-10 ac high voltage power supply at frequencies between 8.0 and 8.1 kHz. Input voltage and input current values were measured by a DL-1540 Yokogawa oscilloscope using a high-voltage (Tektronix P6025) and a low-voltage probe (Yokogawa 70996), respectively. The voltage across a 100 Ω resistor in series with the reactor was used to determine the input current. A voltage is measured, but the oscilloscope reading could be manipulated in a way that displayed the current by taking the resistor into account. The resistor parallel to the reactor was the load resistor, which prevented too much voltage from reaching the reactor. The ac voltage values around 2.600 kV were applied to the electrodes to produce glow discharge plasmas; these voltages were rms (root mean square) voltages.

2.4. Product analysis and characterization

The reaction mixture was continuously monitored with a MKS-UTI PPT quadrupole residual gas analyzer mass spectrometer (MS) with a Faraday cup detector and a variable high-pressure sampling manifold. Samples from the gas stream were taken into a sample loop and analyzed using a Hewlett Packard 5970 series mass selective detector coupled to a Hewlett Packard 5890 Gas Chromatography (GC/MS) equipped with a TCD detector with a HP-1 column (cross-linked methyl siloxane) 12.5 m × 0.2 m × 0.33 μm film thickness. The electrodes used were provided by Dr. Hayashi of Association of Super-advanced Electronics Technologies (ASET) or designed and assembled in our laboratory. Some electrodes were treated in our laboratory; copper and tin and tin oxide particles were deposited onto these electrodes by electroless plating.

Deposits on the electrodes were investigated using a Scintag XDS-2000 diffractometer with Cu Kα X-ray radiation and a Leybold vacuum system equipped with a SPECS multichannel energy analyzer XPS spectrometer with Mg and Al anodes as the X-ray source.

3. Results

3.1. Methane decomposition using different electrodes

The main focus of this investigation was to determine the effect of using different metal inner electrodes on the conversion of methane and the production of hydrogen. The conditions for this reaction were set at 20 ml/min and 2.56 kV input voltage (rms input voltage); pure methane was the reaction gas. The only variable changed during these experiments was the material of the inner electrode. The setup was purged with ultrahigh purity air, and an air plasma was employed to "clean" the electrodes of residues from cleaning and rinsing the electrode before each set of reactions. The reaction was equilibrated at the beginning, and then the power was turned to 2.56 kV to start the decomposition of methane. The power was turned off when the reaction reached an equilibrium level, usually after 30–45 min. This procedure was repeated two times for a total of three runs under plasma conditions to show the reproducibility of the reaction in a short period of time and to observe the course of the reaction over time. After each set of reactions, the setup was purged with air and an air plasma was applied, usually overnight. The used electrodes and the quartz tube were then cleaned using water and acetone.

Very different results were achieved in these reactions. In general, the destruction of methane decreased during the three runs as did the production of hydrogen. The difference between the metal electrodes was seen in the extent the methane decomposition and the hydrogen evolution decreased. Two examples are shown in Fig. 4a and b; the decomposition of methane and hydrogen production is shown in the mass spectra for nickel and for palladium, respectively.

The deactivation of nickel is significant as shown in Fig. 4a. In the case of nickel, as seen in Tables 1 and 2, the methane decomposition dropped from 21.8% in the first run to 7.0% in the third run. The drop in hydrogen production was correlated well with the decrease in methane decomposition and showed a similar drop, from 10.6 vol.% (run 1) to 5.6 vol.% (run 3). A less drastic decrease was observed for the hydrogen production using a palladium inner electrode (Fig. 4b). The hydrogen evolution dropped from 16.5 to 15.2 vol.%. As in the case of nickel, the decomposition of methane showed a similar trend. The decrease in decomposition was almost insignificant, from 21.2% for run 1 to 20.3% for run 3. The changes in the baseline for methane could be due to slight changes in its flow rate and may be by a baseline drift caused by the mass spectrometer itself.

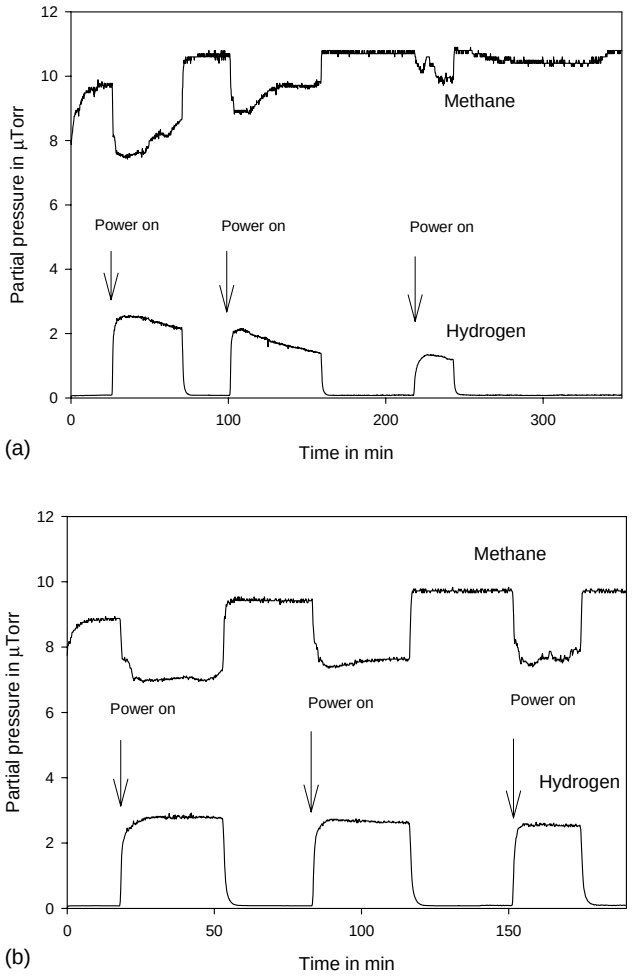

Fig. 4. Mass spectrum of reaction with (a) Ni electrode and (b) Pd electrode showing methane destruction and hydrogen evolution.

The behavior of the different metal inner electrodes used in these experiments is summarized in Tables 1 and 2. It is clearly seen that the choice of the metal for the electrode influenced the conversion of methane and the evolution of

Table 1
Methane decomposition for various metal inner electrodes at 2.56 kV input voltage and 20 ml/min CH_4

Metal	Methane decomposition (run 1) (%)	Methane decomposition (run 2) (%)	Methane decomposition (run 3) (%)
Rh	22.6	23.1	18.8
Ni (coated)	19.9	14.3	10.0
Ni	21.8	12.0	7.0
Pt	22.4	22.9	23.2
Au	20.5	14.6	6.5
Pd	20.5	19.1	22.0
Fe	23.4	22.1	21.2
Cu	18.2	17.4	17.1
Pd (new)	21.2	20.6	20.3
Sn (coated)	18.5	24.6	28.2
Cu (coated)	27.7	21.7	22.4

Table 2
Hydrogen production for various metal inner electrodes at 2.56 kV input voltage and 20 ml/min CH_4

Metal	Hydrogen evolution (run 1) (vol.%)	Hydrogen evolution (run 2) (vol.%)	Hydrogen evolution (run 3) (vol.%)
Rh	12.5	11.0	10.5
Ni (coated)	9.2	7.0	5.7
Ni	10.6	7.7	5.6
Pt	12.5	12.1	11.7
Au	11.2	8.8	6.7
Pd	12.5	12.1	11.3
Fe	13.3	14.5	14.3
Cu	14.5	14.0	13.9
Pd (new)	16.5	15.7	15.2
Sn (coated)	17.4	18.1	18.7
Cu (coated)	13.8	13.5	13.1

hydrogen. The electrodes seemed to deactivate during the three runs, but the degree of deactivation is different for each individual metal. The decomposition (or percentage of conversion) is usually in a range from 20 to 30%. Both nickel electrodes, one of them electroplated commercially and the other one coated with nickel nanoparticles by spraying a sol and then heating, showed almost the same decline in decomposition and evolution, as did the gold electrode, which appeared very corroded after the reactions.

The conversion of methane dropped by 1–5% for most other metals and the evolution of hydrogen was lowered by 1–2 vol.% in most cases over a period of 3 h with measurements based on the MS results. The deactivation affected the decomposition of methane more than the production of hydrogen. The exception was the electrode coated with tin and tin oxide by electroless plating requiring no electrical energy. This electrode showed increasing ability to decompose methane in the three runs, but also exhibited a slight increase in the production of hydrogen. In the case of the iron electrode, both parameters were almost constant, but the hydrogen production dropped significantly in the fourth run, not shown in Table 2, down to 11.5 vol.%, probably due to coking. The electrode coated with copper nanoparticles by electroless plating showed similar behavior as the solid copper electrode with respect to hydrogen production, but the coated electrode decomposed methane more effectively than the solid electrode did. The two palladium electrodes showed very similar trends in their ability to decompose methane, whereas the "newer" electrode yielded a higher hydrogen production compared to the "older" electrode. These electrodes might be from different sources (different manufacturers and different make) and might have a different core material onto which the palladium was coated, for the "newer" electrode it was copper. Palladium, platinum, and the tin/tin oxide coated electrodes showed the best overall performance with a high rate of methane decomposition but at the same time still yielded significant amounts of hydrogen. These three electrodes also exhibited the least deactivation of all the tested inner electrodes. Reversing the polarity of the electrodes, making the inner electrode the ground electrode, caused no change in decomposition or evolution in the case of gold.

Table 3
Influence of cleaning the Pd inner electrode on methane decomposition at 2.56 kV input voltage and 20 ml/min CH_4

Electrode	Methane decomposition (run 1) (%)	Methane decomposition (run 2) (%)	Methane decomposition (run 3) (%)
Pd (new)	21.2	20.6	20.3
Pd (cleaned)	22.4	20.4	20.2
Pd (not cleaned)	14.5	15.9	14.0

3.2. Cleaning the electrodes and methane decomposition

The influence of cleaning the electrodes (as described above) on the decomposition of methane and the evolution of hydrogen was investigated in the following experiments whose results summarized are in Tables 3 and 4. The fresh and the cleaned electrode showed methane decomposition of comparable magnitude. The hydrogen evolution, however, was significantly lower when these two cases were compared; the hydrogen production dropped by about 3 vol.%. When this electrode was used again, but this time without cleaning, a very significant drop in activity was observed. The decomposition rate dropped by 6–8% depending on the run number, and furthermore, the hydrogen production decreased accordingly. The drop in hydrogen evolution was less pronounced in the first run exhibiting a value closer to one of the case when the electrode was cleaned. In the second and third run, however, significant differences were observed in the degree of hydrogen production; the values differed by about 3 vol.%.

3.3. Effect of flow rate on methane decomposition and hydrogen evolution

The effect of altering the input flow rate on the hydrogen production and methane decomposition was studied in this set of experiments. The flow rate was varied between values of 10 and 140 ml/min; all other parameters such as the input voltage were left unchanged in these reactions. The values reported here are the average values of three runs, as before. In these runs, the decomposition rates and evolution rates were similar to the average rates. A similar trend was

Table 4
Influence of cleaning the Pd inner electrode on hydrogen production at 2.56 kV input voltage and 20 ml/min CH_4

Electrode	Hydrogen evolution (run 1) (vol.%)	Hydrogen evolution (run 2) (vol.%)	Hydrogen evolution (run 3) (vol.%)
Pd (new)	16.5	15.7	15.2
Pd (cleaned)	13.6	13.1	11.9
Pd (not cleaned)	12.9	10.2	8.5

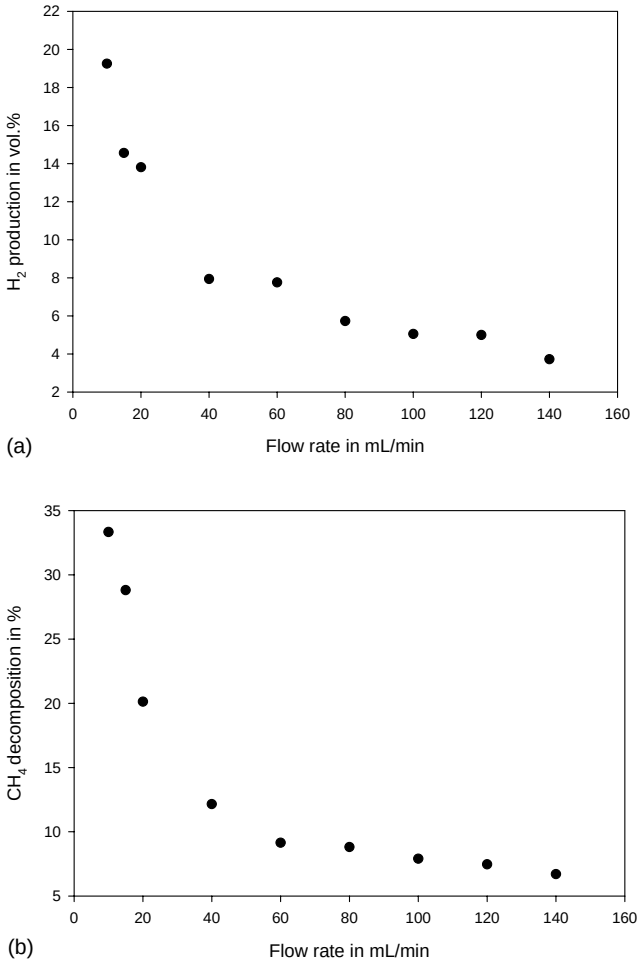

Fig. 5. (a) Hydrogen production (vol.%) and (b) methane decomposition in % using a feed methane at various flow rates and 2.56 kV.

observed in the decomposition of methane and in the evolution of hydrogen, as shown in Figs. 5 and 6. The hydrogen production showed an exponential decline with a maximum conversion at low flow rates (Fig. 5a). The maximum hydrogen evolution achieved was 19.5 vol.% at a flow rate of 10 ml/min, and the hydrogen production seemed to level off at around 4 vol.% at higher flow rates. The decomposition of methane exhibited the same exponential decline, as was observed for the hydrogen production (Fig. 5b). The decomposition rate was high at low flow rates and decreased to an almost constant value at high flow rates, at about 6–7% decomposition at flow rates of over 100 ml/min. The highest decomposition rate (or percentage of conversion) in this study of about 33% was achieved at a low flow rate of 10 ml/min.

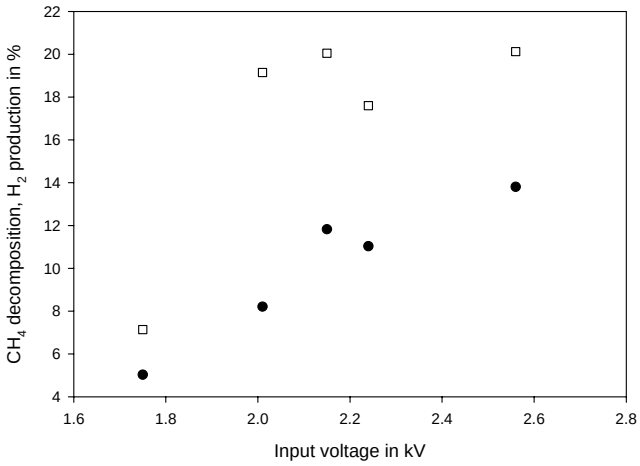

Fig. 6. Methane decomposition in % and hydrogen evolution in vol.% using a feed of 20 ml/min methane at various input voltages.

3.4. Effect of input voltage on methane decomposition and hydrogen evolution

In this study, the influence of the input voltage on the methane decomposition rate and the hydrogen production was investigated. As before, the values represented here are average values from three consecutive runs. The hydrogen evolution and the methane decomposition showed different trends (Fig. 6). The hydrogen evolution showed a nearly linear trend with increasing input voltage. The hydrogen production increased from about 5 vol.% at 1.75 kV input voltage to 14 vol.% at 2.56 kV. The decomposition of methane, however, exhibited a very dissimilar behavior. The decomposition rate increases from a very low value of 7% at an input voltage of 1.75 kV to a plateau of about 18–20% at voltages over 2.0 kV. It seemed that the decomposition above this threshold is independent of an increase in applied input voltage.

3.5. Mass spectroscopic studies

Investigation of the products of the methane decomposition by mass spectrometry and by GC/MS was the main purpose of this part of the study. The mass spectra of the reaction products are shown in Fig. 7 and compared to the spectra with the power off in Fig. 8. The mass spectra when the power was off, taken after a reaction was run, showed that predominately methane with an *m*/*z* ratio of 16 and associated peaks at *m*/*z* ratios of 14 and 15 were present. Other major peaks in this spectrum were assigned to hydrogen radicals and hydrogen at *m*/*z* ratios of 1 and 2, respectively, to alkane species at *m*/*z* ratios of 27, 28 and 29 (major peak), and to the corresponding higher peaks at *m*/*z* ratios of 40 and 42, 56 and 58, and higher *m*/*z* ratios in periodic distances of 14 amu. These peaks are also apparent in the spectrum when the power was off, but in this case, their intensity is lower. These peaks appear in this spectrum because it was taken shortly (15–30 min) after a reaction and residues of this reaction seemed to be present afterwards. This time period is long compared to the residence time which is of the order of a few minutes.

Under plasma conditions, the peaks which were weak in the aforementioned spectrum are much more intense in this spectrum (Fig. 8). The hydrogen peak at an *m*/*z* of 2

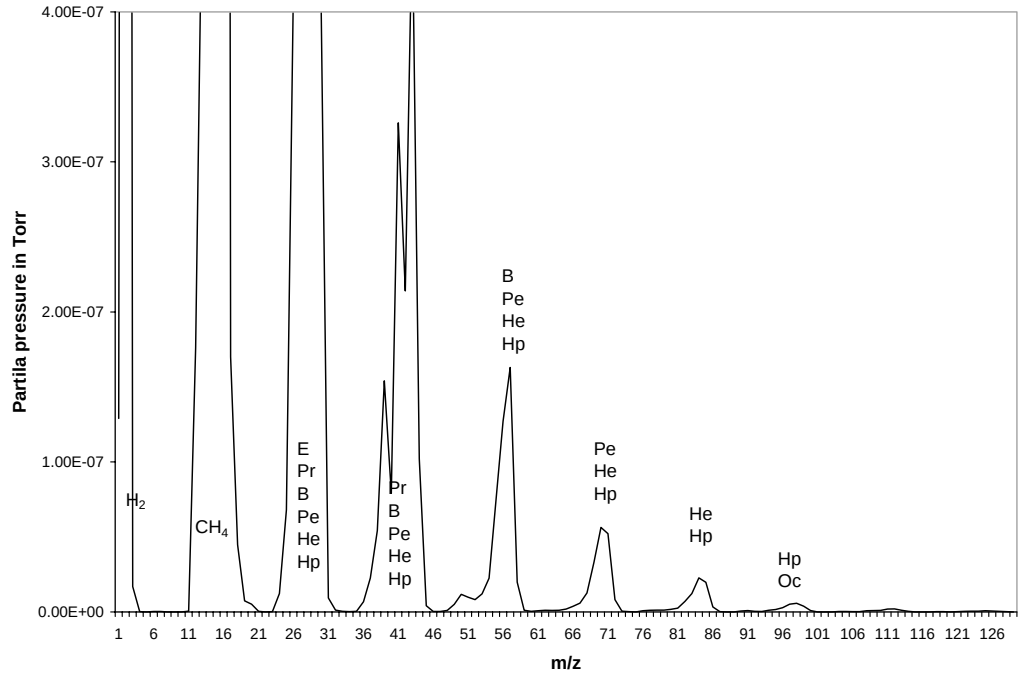

Fig. 7. Mass spectrum of methane decomposition reaction with power 'ON' at room temperature with Pd electrode. The coding is as follows: ethane (E), propane (Pr), butane (B), pentane (Pe), hexane (Hx), heptane (Hp), and octane (Oc).

is more intense than in the other spectrum, whereas the methane peak is decreased according to its decomposition. The peaks centered around an *m*/*z* of 28 could be attributed to alkane species such as ethane (E), propane (Pr), butane (B), pentane (Pe), hexane (Hx), and heptane (Hp) and their isomers, but also can be part of systems from cycloalkanes and alkenes. The group of peaks with *m*/*z* ratios of 37, 39 and 41 was assigned to the same species as above with the exception of ethane. Peaks at higher *m*/*z* ratios are due to higher alkanes and their isomer and the corresponding

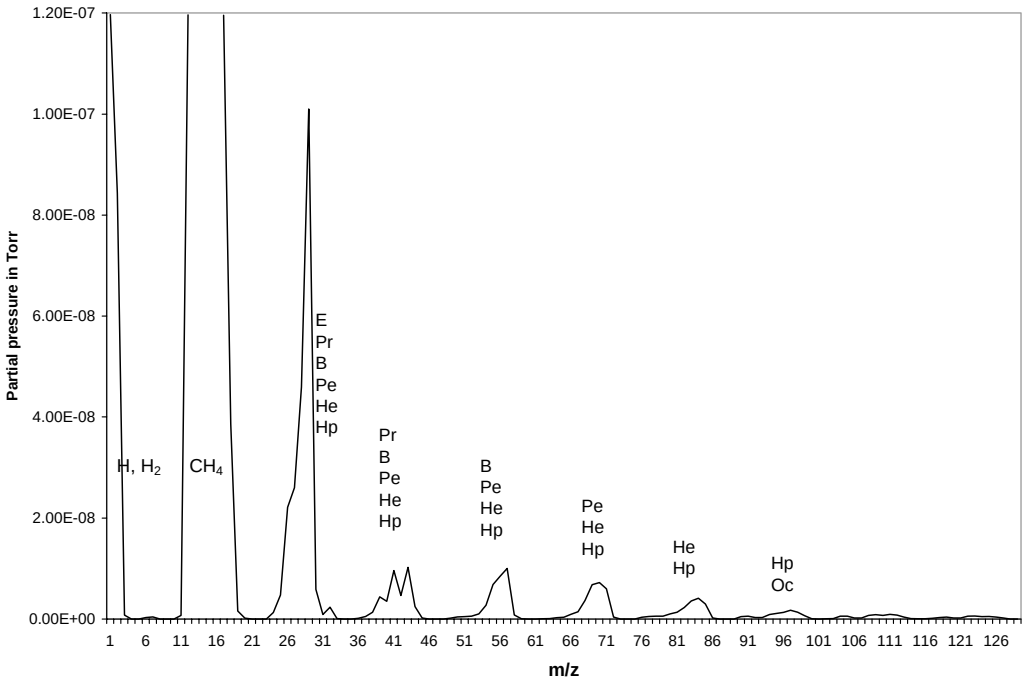

Fig. 8. Mass spectrum of methane decomposition reaction with power 'OFF' at room temperature with Pd electrode. The coding is as follows: ethane (E), propane (Pr), butane (B), pentane (Pe), hexane (Hx), heptane (Hp), and octane (Oc).

Table 5
Compounds found in the GC/MS analyses of samples taken under plasma conditions

2-Methyl propane	2-Methyl-1-propene	Methyl cyclopentane
2-Methyl-1-pentene	3-Methyl-*Z*-2-pentene	2,3,4-Trimethyl-*E*-hexane
2,2,3-Trimethyl hexane	2,3-Dimethyl pentane	3,3,4-Trimethyl hexane
2,3,5-Trimethyl hexane	1-Propene	2-Butene-*E*
2-Pentene	3-Methyl pentane	2-Methyl pentane
cis-1,2-Dimethyl cyclopropane	*trans*-1,2-Dimethyl cyclopropane	2-Methyl-2-butene

cycloalkanes and alkenes. The peaks around an *m*/*z* of 57 could be caused by the alkanes, butane, pentane, hexane, heptane, octane and higher alkanes, as well as isomers of these such as 2,2-dimethyl pentane, 2-methyl hexane and 3-methyl pentane. Alkenes such as 2-methyl-1-pentene have to be accounted for as well when assigning these peaks.

In the resulting spectra from the GC/MS analysis of samples taken under plasma conditions, a multitude of compounds were found as listed in Table 5. The main products of the reaction, ethane and lower alkanes were not listed in this table as well as hydrogen and methane because it was difficult to distinguish them from the higher hydrocarbons in the spectra, but they are clearly present as shown by the mass spectrometric analysis. The species listed here were the major species observed in the spectra obtained using the GC/MS and gave the best quality agreement when assigning them with the GC/MS software. This list is not complete because numerous minor peaks are present and due to the multitude of species present, it was very difficult to identify these species. It can be seen from Table 5 that the major species are branched alkanes and alkenes as well straight alkenes and substituted cycloalkanes.

3.6. Characterization of electrodes and electrode deposits

Collection of the X-ray diffraction patterns of the copper and tin/tin oxide coated electrodes were performed, and the patterns are shown in Fig. 9a and b. In the pattern for the copper coated electrode, no copper oxides were observed. The pattern matches those of copper metal and carbon having a diamond structure, as shown in Fig. 9a. In the case of the tin/tin oxide coated electrode, the same carbon species can be identified again (Fig. 9b). However, the assignment of the tin and tin oxide species is a bit more complicated. The only patterns that match the shown pattern are that of tin metal and that of β-tin oxide (SnO). Compared to the patterns from the database, several strong peaks are missing which could be due to preferential orientation of the spherical electrode in the diffractometer and the way the electrode was prepared.

No useful information was gained from the analysis of the carbon deposits washed off the electrode surface with toluene, because only toluene was detected using the GC/MS. XPS analysis of a palladium electrode coated with carbon deposits yielded only the identity of the palladium metal by observation of the Pd 3d, $3d_{5/2}$ and $3d_{3/2}$ peaks; before the analysis it was known that the electrode was either palladium or platinum coated. Furthermore, the carbon C 1s peak was identified, but no conclusion could be drawn about the nature of the carbon species, whether it was aromatic or aliphatic carbon deposited on the surface of the palladium electrode. A carbon balance was not attempted due to the nature of the setup which makes it difficult to collect the solid deposits but will be tried in future studies.

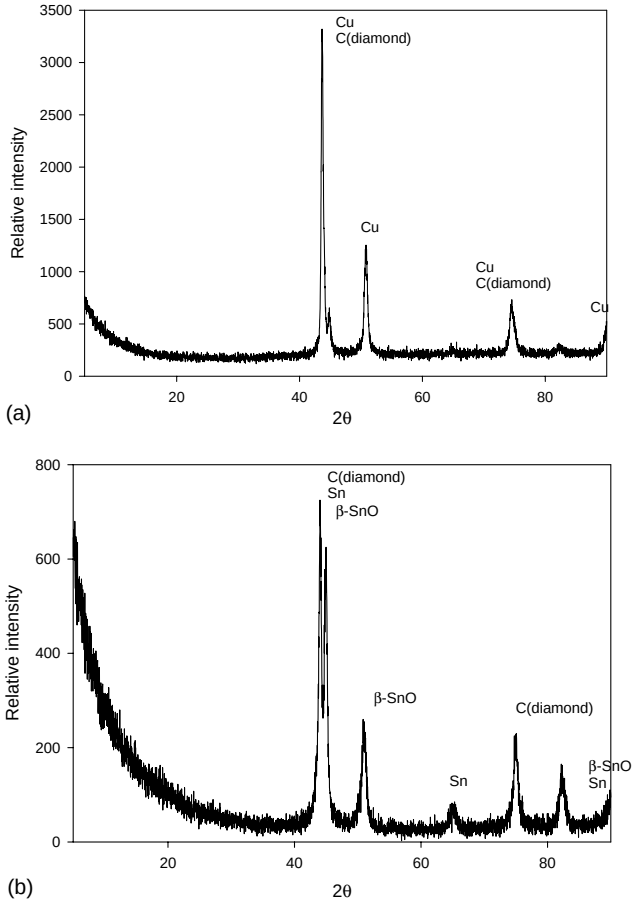

Fig. 9. X-ray diffraction pattern of (a) copper coated electrode and (b) tin/tin oxide coated electrode.

4. Discussion

4.1. Metal effect

The metal effect in the water splitting reaction was described by Luo et al. [22]. Oxygen radicals passivated the surface of the metal and depending on the reactivity of the metal with oxygen, surface oxides were formed. Stable metals, therefore, showed higher activities for water splitting. In the carbon dioxide reforming of methane, a difference in

deactivation was observed. Nickel catalysts were effective in these reactions, but rapid deactivation from coking limited their efficiencies [23,24]. Noble metal catalysts such as platinum catalysts showed a reduction in coking, and therefore, a prolonged period of activity [25–28].

In the study of methane decomposition, similar trends were observed. The noble and unreactive metals such as platinum, rhodium and palladium showed high decomposition and hydrogen evolution activities in these reactions and deactivation was relatively low. The decomposition ability of platinum is slightly higher than that of palladium, but palladium showed higher conversion for hydrogen than platinum. The reason might lie in the different effect of coking on the hydrogen evolution and in a higher catalytic activity of palladium. Ordóñez et al. [29] observed more pronounced deactivation of a platinum catalyst compared to a palladium catalyst due to coking. Gold is also a member of the noble metal class, but showed significant deactivation in the decomposition reaction, which resulted in low hydrogen evolution. Initial activity of gold was almost as high as those of palladium and platinum, however, its activity dropped off sharply in the next two runs. The major deactivation was likely caused by a combination of sintering of the electrode, as evident in the corroded appearance of the electrode after the reaction and coking. Avgouropoulos et al. [30] observed a significant deactivation of gold catalysts compared to copper and platinum catalysts in the selective oxidation of carbon monoxide. Other authors attributed this loss in activity to sintering and coking [31,32]. Copper, as a less reactive metal, also yielded high decomposition rates as well as high hydrogen evolution efficiencies. The higher decomposition rate for the copper coated electrode might be due to the higher surface area of the copper nanoparticles on the electrode. The deactivation of the nickel electrode seemed to be due to a combination of coking and the increased reactivity of the electrode. Similar behavior would be expected for the reactive iron electrode, but it seemed its reactivity in the methane reaction with the reaction products was suppressed. The high and increasing activity of the tin/tin oxide electrode might be due to the presence of oxygen in tin oxide. The observed dependence of the decomposition of methane on the electrode surface material when all other parameters are kept the same indicates that the surface and probably surface effects play a role in this decomposition reaction apart from the influence of the plasma. The temperature of the reactor is not much higher than room temperature (up to 60 °C), but the electron temperature is of the order of 10,000 K.

4.2. Methane decomposition

The reaction to coke and hydrogen seemed to be thermodynamically preferred in the decomposition of methane. Mass spectrometric data suggested that the formation of other compounds such as alkanes, alkanes and cycloalkanes occurred as well. This conclusion was based on the appearance of peaks other than those of methane and hydrogen in above mentioned mass spectra. The presence of other compounds was confirmed by analyzing samples using the GC/MS. Species found included ethane and ethylene, part of the major system around the *m*/*z* ratio of 28, and analogous hydrocarbons in a system with 12–13 mass units spacings in between them, as is typical for methyl and methylene groups. The system around an *m*/*z* of 41, for example, contained peaks for propane and higher alkanes, which showed this *m*/*z* value in their individual mass spectra due to fragmentation.

For the decomposition of methane, a mechanism can be suggested (Eqs. (1)–(17)). Decomposition mechanisms were investigated in our research group before especially in the case of chlorofluorocarbons [33,34] and this mechanism is based on these insights. The mechanism is initiated by electron activation of methane and shows the formation of coke, hydrogen and alkanes, alkenes (which will react further with alkyl radicals to form branched alkanes) and cycloalkanes. The mechanism considered reactions initiated in the gas phase by the influence of the plasma; radical reactions outside the plasma were believed to be recombinations and possibly chain polymerization, and the formation of gas phase free radicals in the absence of plasma seemed minor. The formation of aromatic compounds seemed probable. The form of coke observed on the electrodes might be diamond-like as seen in the X-ray diffraction pattern shown before. This mechanism is based on observations in the mass spectra and the results for the samples analyzed with the GC/MS. The collisions for the formation of higher hydrocarbons such as propane and butane as shown in Eq. (12) and higher are simplified and might be the result of sequential collisions. The surface plays a role in the initiation of the radical reaction and is also important in the recombination and termination reactions.

$$CH_4 + e^- \rightarrow CH_4{}^*/CH_4{}^{*+} \quad (1)$$

$$CH_4{}^*/CH_4{}^{*+} \rightarrow \mathbf{CH_3^\bullet}/CH_3{}^{\bullet+} + \mathbf{H^\bullet} \quad (2)$$

$$CH_3{}^\bullet/CH_3{}^{\bullet+} + CH_4{}^*/CH_4{}^{*+} \rightarrow CH_4 + CH_3{}^{\bullet*}/CH_3{}^{\bullet*+} \quad (3)$$

$$CH_3{}^{\bullet*}/CH_3{}^{\bullet*+} \rightarrow CH_3{}^{\bullet*+}/CH_3{}^{\bullet*+} \quad (4)$$

$$CH_2{}^\bullet/CH_2{}^{\bullet+} + CH_4{}^*/CH_4{}^{*+} \rightarrow CH_4 + CH_2{}^{\bullet*}/CH_2{}^{\bullet*+} \quad (5)$$

$$CH_2{}^{\bullet*}/CH_2{}^{\bullet*+} \rightarrow \mathbf{CH^\bullet}/CH^{\bullet+} + \mathbf{H^\bullet} \quad (6)$$

$$CH^\bullet/CH^{\bullet+}CH_4{}^*/CH_4{}^{*+} \rightarrow CH_4 + CH^{\bullet*}/CH^{\bullet*+} \quad (7)$$

$$CH^{\bullet*}/CH^{\bullet*+} \rightarrow \mathbf{C^\bullet}/C^{\bullet+} + \mathbf{H^\bullet} \quad (8)$$

$$2H^\bullet \rightarrow H_2 \quad (9)$$

$$2CH_3{}^\bullet \rightarrow CH_3CH_3 \quad (10)$$

$$2CH_2{}^\bullet \rightarrow CH_2CH_2 \quad (CH_2CH_2 \text{ will react further}) \quad (11)$$

$$2CH_3^\bullet + CH_2^\bullet \rightarrow CH_3CH_2CH_3 \quad (12)$$

$$CH_3^\bullet + CH_2^\bullet + CH^\bullet \rightarrow CH_2CHCH_3 \quad (CH_2CHCH_3 \text{ will react further}) \quad (13)$$

$$2CH_3^\bullet + 2CH_2^\bullet \rightarrow CH_3CH_2CH_2CH_3 \quad (14)$$

$$3CH_2^\bullet \rightarrow CH_2CH_2CH_2(\text{cyclic}) \quad (15)$$

$$2CH_3^\bullet + CH^\bullet + CH_2^\bullet \rightarrow CH_3CHCH_2CH_3 \quad (16)$$

$$2CH_3^\bullet + CH^\bullet + 2CH_2^\bullet \rightarrow CH_3CHCH_2CH_2CH_3 \quad (17)$$

4.3. Effect of flow rate, input voltage and electrode cleaning

A drop almost in a negative exponential fashion similar to the trends seen in the water splitting reactions involving methane is observed in the plots of hydrogen production versus flow rate and the methane decomposition versus flow rate. The same reasoning can be used to explain this phenomenon. The residence time decreased as the flow rate increased, and therefore, the time the reactant was in contact with the plasma and the electrode was lower, and there was not enough time for a multitude of reactions to take place. The residence time is of the order of tens of seconds at higher flow rates and around 1 min or more at lower flow rates. The average kinetics of the reaction was slower than the contact time in the case of high flow rates.

The effect of cleaning of the electrode was evident in the influence of coking on the decomposition of methane and the evolution of hydrogen. The coke produced in the reactions deposited on the electrodes and decreased the conversions. Furthermore, this showed that the metal acted catalytically in these reactions because when the electrodes are covered with coke, deactivation occurred, and the decomposition rate and the hydrogen evolution dropped.

The influence of the applied input voltage is best described in terms of energetic electrons. The higher the input voltage was, the higher was the energy input into the plasma. This caused more electrons to have the appropriate energy to excite methane and induced the ionization and decomposition of methane as proposed in the reaction scheme. This influence was clearly seen in the dependence of the hydrogen evolution on the applied input voltage, which followed a linear trend in this case. This can be understood in terms of the electrons inducing more efficient breakup of methane and the increased production of hydrogen radicals which then formed hydrogen molecules. Methane decomposition, however, showed a different behavior. The increase in input voltage induced higher decomposition rates up to a value of about 2 kV. Above this value, the decomposition rates seemed independent of the applied input voltage. This indicated that a certain energy was necessary to induce efficient breakup of methane, and above this energy, an increase in input voltage, and therefore, electron energy did not influence the methane breakup efficiency anymore.

5. Conclusions

In this research, the effect of using different metal electrodes on the methane decomposition and hydrogen evolution was investigated. Noble metals such as palladium and platinum showed the highest decomposition rates and highest hydrogen evolution as well as the lowest deactivation. Significant deactivation was observed for nickel and gold electrodes due to reactivity with reaction products, coking and sintering. Electrodes coated with copper nanoparticles and tin/tin oxide nanoparticles showed high activity. In the case of the copper coated electrode, the activity was comparable to the activity of the electroplated copper electrode, but the decomposition rate of methane was slightly higher probably due to the characteristics of the coating.

Several other factors influencing the methane decomposition and hydrogen evolution were also studied. The flow rate has a significant impact on both the methane decomposition and the hydrogen evolution. With increasing flow rate, the decomposition rate and the hydrogen production showed a negative exponential decline due to the decreased residence time in the plasma zone. Cleaning the metal electrode had a profound impact on the methane decomposition due to coking and indicated that there was a catalytic role of the electrode in these reactions. Increasing applied input voltage increased the hydrogen production and the methane decomposition up to a threshold value by supplying more energetic electrons. Other major products apart from hydrogen are lower and higher alkanes, alkenes, and cycloalkanes. Branched alkanes were also detected. A reaction scheme accounting for the reaction products was proposed based on the data gathered by using mass spectrometry and analysis of samples using the GC/MS.

References

[1] Uses of Natural Gas, NaturalGas.org, March 2003. http://www.naturalgas.org/overview/uses.asp.
[2] United Nations Framework Convention on Climate Change, Vital Climate Graphics: Climate Change, March 2003. http://www.grida.no/climate/vital/index.htm.
[3] Fuel Cells 2000's Frequently Asked Questions, Fuel Cells 2000, March, 2003. http://www.fuelcells.org/fcfaqs.htm.
[4] J.R. Rostrup-Nielsen, in: J.R. Anderson, M. Boudart (Eds.), Catalytic Steam Reforming Catalysis, Science & Technology, vol. 5, Springer, Berlin, 1984.
[5] D. Wang, S. Czernik, E. Chornet, Energy Fuels 12 (1998) 19–24.
[6] L. Pino, V. Recupero, S. Beninati, A.K. Shukla, M.S. Hegde, B. Parthasarathi, Appl. Catal. A 225 (2002) 63–75.
[7] S. Licht, B. Wang, S. Mukerji, T. Soga, M. Umeno, H. Tributsch, Int. J. Hydrogen Energy 26 (2001) 653–659.
[8] S. Licht, S. Ghosh, H. Tributsch, S. Fiechter, Sol. Energy Mater. Sol. Cells 70 (2002) 471–480.
[9] Z. Zou, J. Ye, K. Sayama, H. Arakawa, Nature 414 (2001) 625–627.
[10] R. Abe, K. Sayama, K. Domen, H. Arakawa, Chem. Phys. Lett. 344 (2001) 339–344.
[11] H. Harada, C. Hosoki, A. Kudo, J. Photochem. Photobiol. A 141 (2001) 219–224.

[12] E. Miller, R. Rocheleau, in: Proceedings of the 2001 US DOE Hydrogen Program Review, Baltimore, MD, US, 2001, pp. 359–381.
[13] G. Hitoki, T. Takata, S. Ikeda, M. Hara, J.N. Kondo, M. Kakihana, K. Domen, Catal. Today 63 (2000) 175–181.
[14] A. T-Raissi, in: Proceedings of the 2001 US DOE Hydrogen Program Review, Baltimore, MD, US, 2001, pp. 879–905.
[15] J. Lee, E. Greenbaum, in: Proceedings of the 2001 US DOE Hydrogen Program Review, Baltimore, MD, US, 2001, pp. 31–44.
[16] L. Bromberg, D.R. Cohn, A. Rabinovich, N. Alexeev, in: Proceedings of the 1998 US DOE Hydrogen Program Review, Baltimore, MD, US, 1998, pp. 627–639.
[17] O. Mutaf-Yardimci, A.V. Saveliev, A.A. Fridman, L.A. Kennedy, Int. J. Hydrogen Energy 23 (1998) 1109–1111.
[18] D. Liu, Y. Xu, X. Yang, S. Yu, Q. Sun, A. Zhu, T. Ma, Diamond Relat. Mater. 11 (2002) 1491–1495.
[19] T. Nozaki, Y. Kimura, K. Okazaki, in: Proceedings of the 16th ESCAMPIG and Fifth ICRP Joint Conference, 14–18 July 2002, Grenoble, France, pp. 37–38.
[20] S.L. Brock, T. Shimojo, S.L. Suib, Y. Hayashi, H. Matsumoto, J. Res. Chem. Intermed. 28 (2002) 13–24.
[21] A. Huang, G. Xia, J. Wang, S.L. Suib, Y. Hayashi, H. Matsumoto, J. Catal. 189 (2000) 349–359.
[22] J. Luo, S.L. Suib, Y. Hayashi, H. Matsumoto, J. Res. Chem. Intermed. 26 (2000) 849–874.
[23] G.Q. Lu, S. Wand, CHEMTECH, 1999, 37–43.
[24] E. Ruckenstein, Y.H. Hu, J. Catal. 162 (1996) 230–238.
[25] A.T. Ashcroft, A.K. Cheetham, M.L.H. Green, P.D.F. Vernon, Nature 352 (1991) 225–226.
[26] V.A. Tsipouriari, A.M. Efstathiou, X.E. Verykios, J. Catal. 161 (1996) 31–42.
[27] M.C.J. Bradford, M.A. Vannice, J. Catal. 173 (1998) 157–171.
[28] S.M. Stagg, E. Romedo, C. Padro, D.E. Resasco, J. Catal. 178 (1998) 137–145.
[29] S. Ordóñez, F.V. Díez, H. Sastre, Appl. Catal. B 31 (2001) 113–122.
[30] G. Avgouropoulos, T. Ioannides, C. Papadopoulou, J. Natista, S. Hocevar, H.K. Matralis, Catal. Today 72 (2002) 157–167.
[31] G. Wang, W. Zhang, H. Lian, Q. Liu, D. Jiang, T. Wu, React. Kinet. Catal. Lett. 75 (2002) 343–351.
[32] Y.-M. Kang, B.-Z. Wan, Catal. Today 35 (1997) 379–392.
[33] F.-J. Spiess, S.L. Suib, Y. Hayashi, H. Matsumoto, Decomposition of CF_4 by microwave heating, in: Proceedings of the ACS Symposium Series, vol. 852, 2003, pp. 338–350.
[34] F.-J. Spiess, X. Chen, S.L. Brock, S.L. Suib, Y. Hayashi, H. Matsumoto, J. Phys. Chem. A 104 (47) (2000) 11111–11120.